RSC Advances

PAPER

View Article Online
View Journal | View Issue

Cite this: *RSC Adv.*, 2023, **13**, 23728

Construction of composite films using carbon nanodots for blocking ultraviolet light from the Sun†

Yibing Bai,[a] Bin Zhao,[a] Jiaxin Ni,[a] Lianhang Sun,[a] Yuning Wang,[a] Jing Wang,[a] Yu Liu,[a] Shiyan Han, *[a] Fugang Gao[b] and Chunlei Zhang*[a]

Carbon nanodots (CNDs) which demonstrate concentration-dependent emission and have a photoluminescence quantum yield of 45% were designed. Transparent CND-containing composite films (CND-films), obtained by combining the CNDs with polyvinyl alcohol in different proportions, were shown to block the UV component of sunlight. Whereas the pure PVA film could not block UV light, the ability of CND-films to block UV light could be adjusted by altering the proportion of CNDs in the film. The larger the proportion of CNDs, the greater the extent of UV blocking. CND-film containing 32 wt% CNDs completely blocked UV light (≤400 nm) from sunlight, without affecting the transmission of visible light (>800 nm). The ability of the CND-films to block the UV component of sunlight was investigated using a commercially available UV-induced color change card, which confirmed that the capacity of the CND-films to block UV light could be adjusted by altering the proportion of CNDs in the film. This study shows that CNDs with concentration-dependent long wavelength emission characteristics can be used as optical barrier units for the preparation of materials to block high-energy short wavelength light.

Received 19th June 2023
Accepted 2nd August 2023

DOI: 10.1039/d3ra04123a

rsc.li/rsc-advances

Introduction

Long-term ultraviolet (UV) exposure can cause many problems, such as eye and skin lesions,[1–3] food deterioration,[4–6] wood surface color change,[7,8] *etc.* Therefore, research into UV blocking has been widely conducted by scholars.[9] With the development of UV blocking materials, carbon nanodots (CNDs) have gradually been used to block high-energy short wavelength light due to their excellent optical absorption and conversion properties.[1,2,10,11] CNDs are a new type of carbon nanomaterial with a particle size <10 nm, excellent resistance to photobleaching and good responsiveness to changes in pH and temperature,[12–16] which are widely used in white light emitting diodes (WLEDs),[17–20] in anti-counterfeiting applications,[21,22] as probes,[23–25] and catalysts,[26,27] and for biological imaging.[28,29] Among the many possible sources of carbon for preparing carbon dots, natural resources and derivatives are particularly attractive because of their abundance, low price, environmental friendliness and sustainability.[30–33] More generally, interest in natural resources and their derivatives as sources of carbon has gradually increased over recent years.[11,21,34–36] Chitin is a natural biopolymer with wide sources and abundant reserves,[37,38] and its deacetylation product, chitosan, is widely utilised because of its abundant reserves, non-toxicity, good biocompatibility, and ease of biodegradation[39] and its use as a source of carbon has been gradually developed.[17] Polyvinyl alcohol (PVA) is a biodegradable, water-soluble, low-cost, film-forming and stable polymer, which has the potential to replace non-biodegradable polymers.[40] Therefore, in this study, we used abundant chitosan as the carbon source and ethylenediamine as the passivator to prepare CNDs that produce concentration-dependent emission, with a photoluminescence quantum yield (PLQY) of 45%. The CNDs were mixed with PVA to prepare CND-based composite films (CND-films) (Scheme 1a). The CND-films can prevent damage caused by exposure to UV radiation in sunlight by absorbing high-energy short wavelength light and converting it into long wavelength emission (Scheme 1b).

Experimental

Raw materials

Chitosan (99.9%) was purchased from Sinopharm Chemical Reagent Co., Ltd (Shanghai, China). Polyvinyl alcohol (PVA, MW 1750) was purchased from Tianjin Kemeiou Chemical Reagent Co., Ltd (Tianjin, China). Ethylenediamine (99%, AR) and absolute ethanol (AR) were purchased from Kemiou Chemical Reagent Co., Ltd (Tianjin, China). All materials were used directly without further purification. 365 nm and 450 nm LED chips were purchased from Looking Long Technology Co., Ltd (Shenzhen, China).

[a]*Key Laboratory of Bio-Based Material Science & Technology (Northeast Forestry University), Ministry of Education, Harbin 150040, China. E-mail: hanshiyan80@163.com; zhangchunlei@nefu.edu.cn*

[b]*Jiangsu Transline Technology Co. Ltd, Changzhou 213100, China*

† Electronic supplementary information (ESI) available. See DOI: https://doi.org/10.1039/d3ra04123a

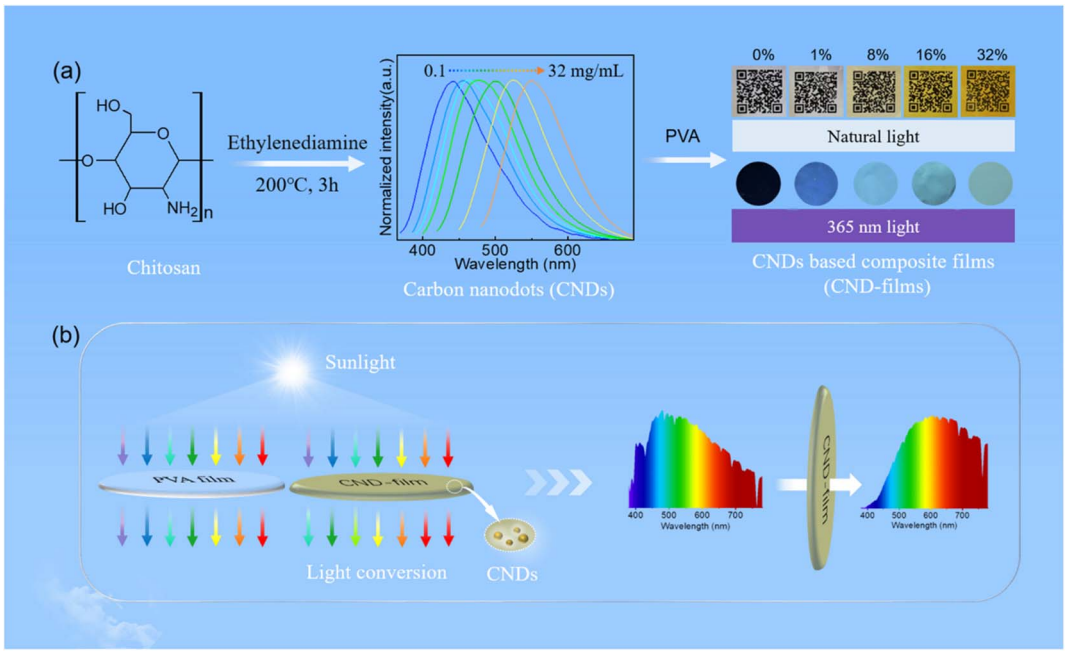

Scheme 1 Schematic illustration of (a) preparation of CNDs and CND-films and (b) blocking of UV light by PVA film and CND-film.

Synthesis of biomass-based carbon dots (CNDs)

Chitosan (0.2 g), ethylenediamine (0.5 mL) and deionized water (10 mL) were mixed in a 50 mL beaker and the mixed solution was then transferred to a 25 mL polytetrafluoroethylene reactor and reacted at 200 °C for 3 h. Once the hydrothermal reaction was complete, the solution was allowed to cool naturally to room temperature and the resulting solution was filtered through a 0.22 μm water-based microporous filter membrane. The filtrate was then freeze-dried to provide the CNDs as a powder.

Preparation of CND-based composite films (CND-films)

A mixture of PVA (1.0 g) and deionized water (25 mL) in a 100 mL beaker was magnetically stirred for 1 h at 95 °C and

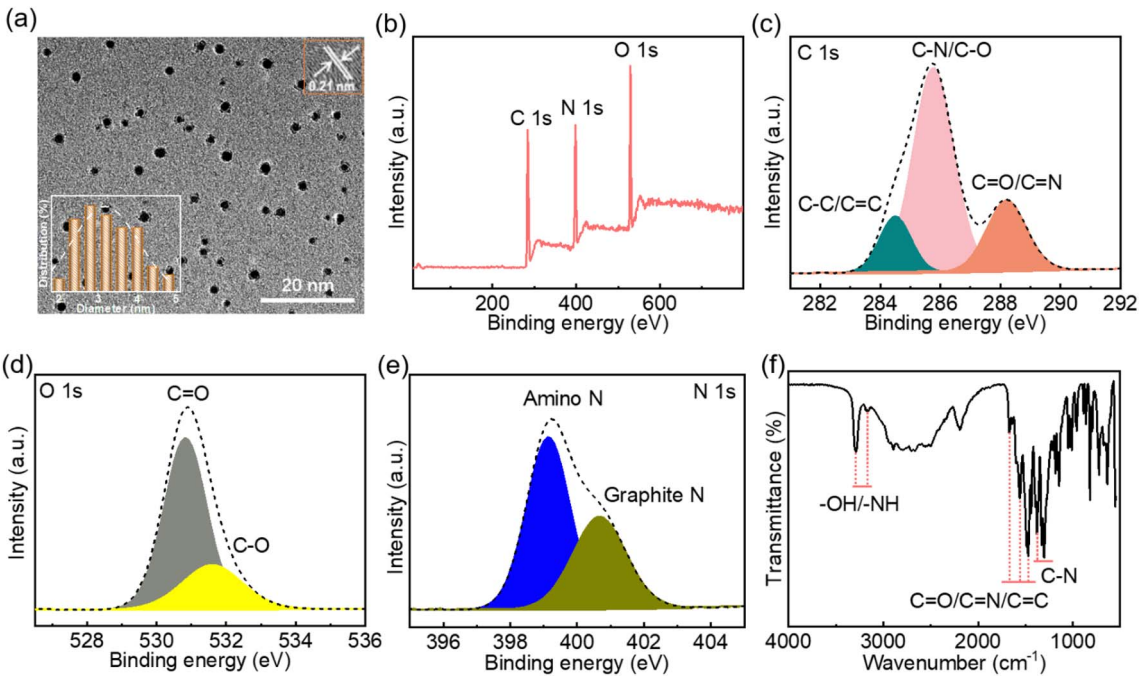

Fig. 1 (a) TEM image of CNDs, inset: high resolution TEM image and particle size distribution; (b) full XPS spectrum of CNDs; (c) C 1s XPS spectrum of CNDs; (d) O 1s XPS spectrum of CNDs; (e) N 1s XPS spectrum of CNDs; (f) FTIR spectrum of CNDs.

then filtered through a 0.22 μm microporous membrane to provide an aqueous solution of PVA. Five pieces of PVA aqueous solutions were prepared under the same conditions, and then 0, 1, 9, 19, 47 mL of CNDs aqueous solution (10 mg mL^{-1}) were added respectively, stirred for 1 h, ultrasonic for 1 h. The mixture was slowly poured into a Petri dish and dried naturally at room temperature to produce the CND-films. CND-films containing 0 wt%, 1 wt%, 8 wt%, 16 wt% and 32 wt% CNDs were prepared using this method.

Fabrication and electroluminescence performance of LED

(1) CND-films containing different proportions of CNDs were cut into circles with diameters of 0.7 cm and the circular pieces of film were used to encapsulate 365 nm semiconductor chips, using epoxy resin as the fixative. The different LEDs were obtained after drying and curing at 40 °C for 12 h.

(2) The WLED produced using CND-films was powered by a universal DC power supply with an operating voltage of 3.0 V and an operating current of 20 mA. An OHSP-350 spectrometer was placed in front of the light source to measure the CIE1931 chromaticity coordinates of the LED.

Test of ability of CND-films to block UV light

The ability of PVA film and CND-films to block UV light was determined using outdoor sunlight as a source of UV light (≤400 nm). The spectra after light conversion through the different films were recorded using an OHSP-350 spectrometer.

Results and discussion

Transmission electron microscopy (TEM) images showed that the as-prepared CNDs have a well-dispersed granular structure (Fig. 1a), with a 0.22 nm lattice (Fig. 1a inset) corresponding to the (100) crystal facet of graphite carbon.[41] The particle diameters of the CNDs are in the range 2–5 nm (Fig. 1a inset), with an average particle size of 3.26 nm. The full X-ray photoelectron

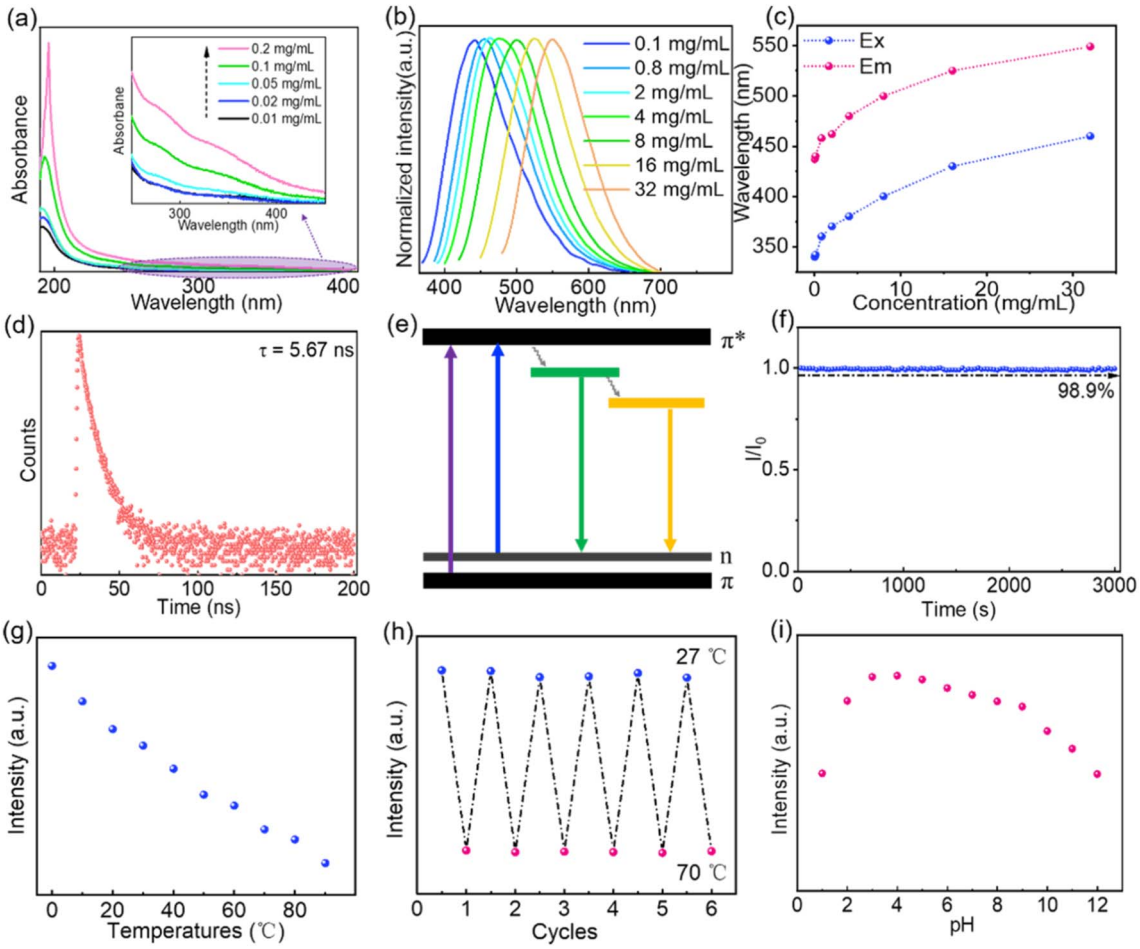

Fig. 2 (a) UV absorption spectra of aqueous solutions of CNDs with different concentrations (0.01–0.2 mg mL^{-1}) (inset: locally enlarged image); (b) normalized emission spectra of aqueous solutions of CNDs with different concentrations (0.1–32 mg mL^{-1}); (c) optimal excitation and maximum emission wavelengths of aqueous solutions of CNDs with different concentrations (0.1–32 mg mL^{-1}); (d) fluorescence decay curve of aqueous solutions of CNDs; (e) schematic illustration showing mechanism of fluorescence emission of CNDs; (f) fluorescence intensity of aqueous solution of CNDs (2 mg mL^{-1}) irradiated (Ex = 365 nm) for 50 min; (g) fluorescence intensity of aqueous solutions of CNDs (2 mg mL^{-1}) at different temperatures (0–90 °C, Ex = 370 nm); (h) fluorescence intensity of aqueous solution of CNDs (2 mg mL^{-1}) on repeated cycling between 27 °C and 70 °C (Ex = 370 nm); (i) fluorescence intensity of aqueous solution of CNDs at different pH (Ex = 370 nm).

spectrum (XPS) indicates that the CNDs contain the elements C (54.22%), N (25.77%) and O (20.01%) (Fig. 1b). Compared with the hydrothermal product formed from chitosan alone, the addition of ethylenediamine to the reaction mixture significantly increases the proportion of N in the CNDs (Fig. S1 and Table S1†). The high-resolution C 1s spectrum (Fig. 1c) of the CNDs shows characteristic peaks at 284.5 eV, 285.8 eV and 288.2 eV, corresponding to C–C/C=C, C–N/C–O and C=O/C=N groups, respectively.[11,42] The high-resolution O 1s spectrum (Fig. 1d) shows characteristic peaks at 530.8 eV and 531.6 eV, which can be attributed to C=O and C–O groups,[43,44] respectively. The high-resolution N 1s spectrum (Fig. 1e) shows characteristic peaks at 399.1 eV and 400.7 eV, corresponding to amino N[17] and graphite N,[45] respectively. These results confirm the formation of a graphitized carbon core. The Fourier-transform infrared (FTIR) spectrum of the CNDs (Fig. 1f) shows the characteristic absorption peaks of –OH/–NH,[46] C=O/C=N/C=C[11,46,47] and C–N (1376 cm^{-1}) bonds,[48] indicating the presence of hydroxyl, amino, carbonyl and other functional groups on the surface of the CNDs. Taken together, the XPS and FTIR spectra confirm that the CNDs have a graphitized carbon core and abundant surface groups.

After structural characterization of the CNDs, we next investigated their optical properties. The UV absorption spectra of aqueous solutions of CNDs with different concentrations are shown in Fig. 2a. As the concentration increases, UV absorption is enhanced and the absorption threshold extends to 400 nm (Fig. 2a inset). This may be caused by aggregation of CNDs at higher concentrations, leading to enhanced π–π* transitions of C=C bonds and n–π* transitions of C=O/C=N bonds.[10,49] The fluorescence emission of aqueous solutions of CNDs is excitation wavelength-dependent (Fig. S2†), which means that short wavelength light is absorbed and converted into longer wavelength emission.[2,10,49] As the concentration of CNDs in the solution increases, the maximum emission redshifts to longer wavelength (Fig. 2b and c) and the corresponding optimal excitation wavelength also redshifts (Fig. 2c), indicating that the emission of the CNDs is concentration-dependent. At low concentrations, as the concentration of CNDs in the aqueous solution increases, aggregation of the CNDs enhances radiative transition, leading to a gradual increase in emission intensity. When the concentration of the solution increases beyond 2 mg mL^{-1} (Fig. S3†), aggregation enhances π–π interactions between carbon cores and aggregation-caused quenching occurs, leading to a decrease in emission intensity.[11,50] Additionally, fluorescence resonance energy transfer (FRET) or reabsorption may be also partially responsible for the decrease in emission intensity.[51,52] The fluorescence decay curve of an aqueous solution of CNDs can be fitted to a double exponential decay lifetime (Fig. 2d and Table S2†), indicating that the CNDs have a double fluorophore composed of a carbon core and a surface fluorophore.[52,53] The fluorescence lifetime of an aqueous solution of CNDs was calculated to be 5.67 ns. The luminescence mechanism of solutions of CNDs with concentration-dependent emission can be interpreted as follows: at low concentrations, the carbon core state dominates, with emission of blue light; as the concentration increases, the surface states become dominant and absorbed short

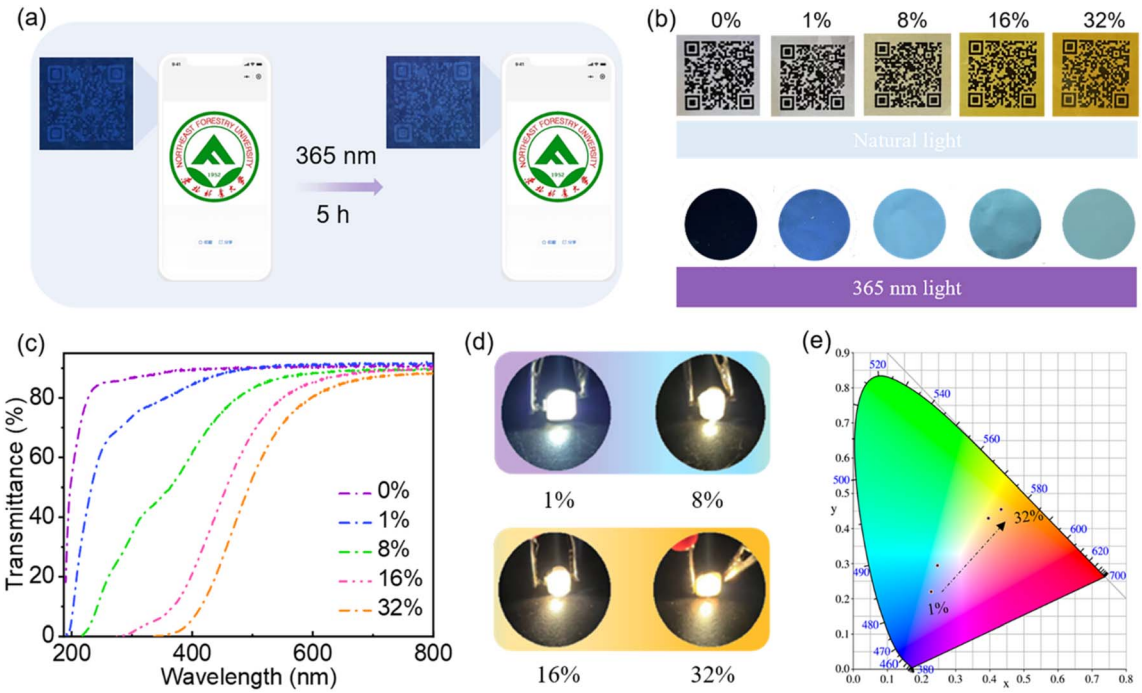

Fig. 3 (a) Fluorescence color photos of QR code pattern printed using solution of CNDs before and after 5 h irradiation with 365 nm light; (b) color photos of CND-films containing different proportions of CNDs under natural and 365 nm light; (c) UV transmittance spectra of different CND-films; (d) photos of different CND-films coated onto 365 nm chip and energized; (e) CIE1931 chromaticity diagram of WLED constructed using CND-films.

wavelength light is converted into long wavelength light emission (Fig. 2e). The absolute PLQY of CNDs is 45%, which is higher than that of the hydrothermal product formed from chitosan alone (4.81%) and also higher than that reported for other carbon dots (Table S3†). These results confirm that the participation of EDA in the reaction can increase the absolute PLQY of CNDs. The optical stability of the CNDs was further analyzed. The fluorescence intensity of an aqueous solution of CNDs only declined by 1.1% following continuous excitement at 370 nm for 3000 s (Fig. 2f), indicating that aqueous solutions of CNDs have good resistance to UV bleaching. Moreover, the CNDs solution was still transparent after being placed indoors for 12 days, and the fluorescence emission did not change (Fig. S4†). The fluorescence emission of aqueous solutions of CNDs was also measured at different temperatures (Fig. S5†). The intensity of fluorescence emission of the solutions gradually decreased as the temperature increased (Fig. 2g) because of decreased radiative transition.[54,55] The intensity of the fluorescence emission of an aqueous solution of CNDs showed a stable recovery after six consecutive cycles of temperature change (Fig. 2h). These results confirm that the fluorescence emission of solutions of CNDs is both stable and reversible. The fluorescence emission spectra of aqueous solutions of CNDs at different pH are shown in Fig. S6.† The fluorescence intensity of an aqueous solution of CNDs decreased significantly under strongly acidic (pH < 3) or strongly basic (pH > 9) conditions but was relatively stable over the pH range 3–9 (Fig. 2i). This is caused by protonation–deprotonation of functional groups on the surface of the CNDs[29,56,57] These results confirm that CNDs not only have tunable emission and stable optical properties, but can also absorb short wavelength light and convert it into long wavelength light emission, thereby preventing damage caused by short wavelength light. Aqueous solutions of CNDs have good optical properties and can thus be used as

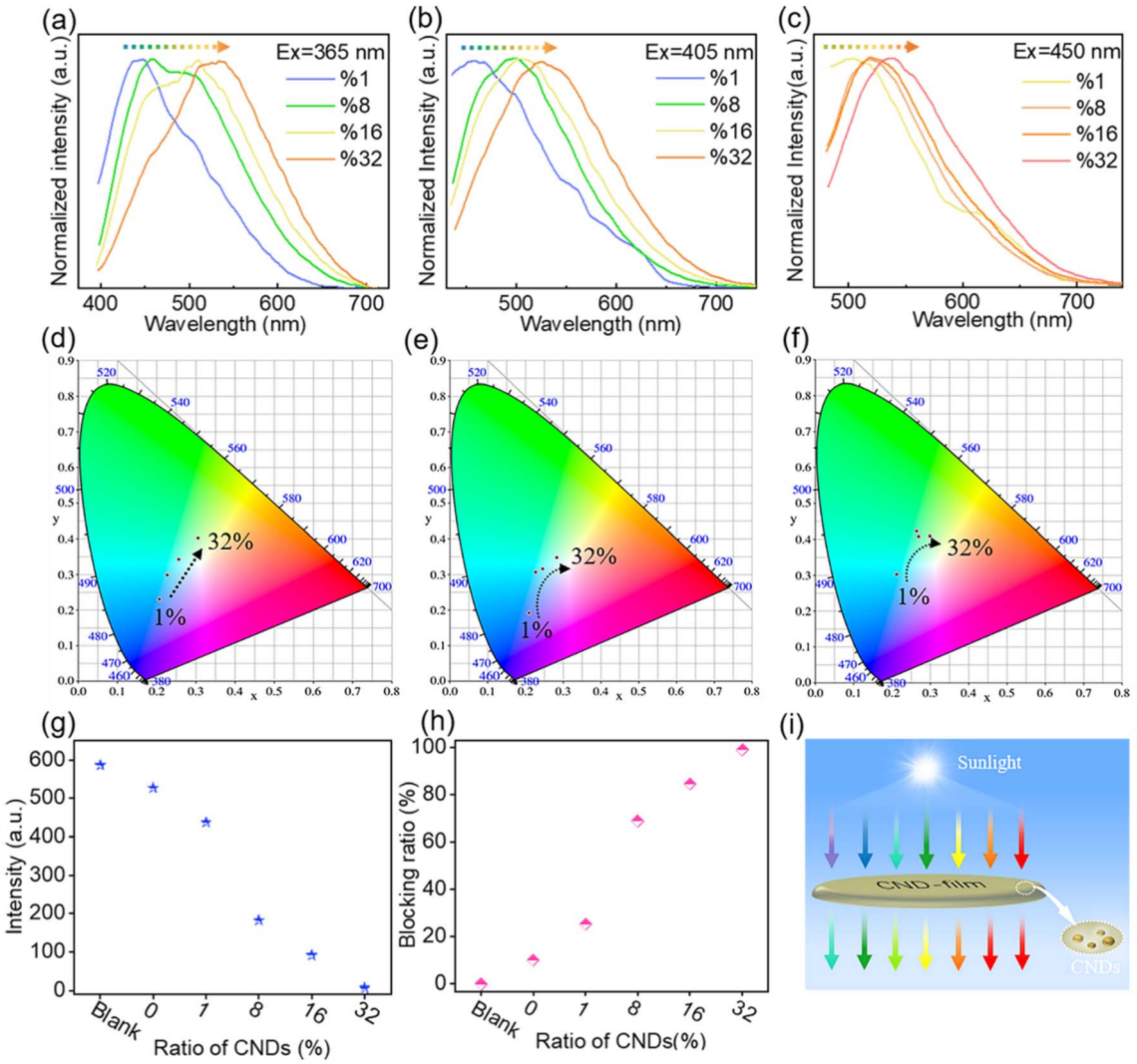

Fig. 4 (a–c) Normalized emission spectra of CND-films (1–32 wt% CNDs) under different wavelength excitation (365 nm, 405 nm and 450 nm); (d–f) CIE (1931) coordinates diagram of CND-films (1–32 wt%) under different wavelength excitation (365 nm, 405 nm and 450 nm); (g) blocking of UV in sunlight (≤400 nm) by different CND-films (0–32 wt%); (h) extent of blocking of UV in sunlight (≤400 nm) by different CND-films (0–32 wt%); (i) schematic showing mechanism of blocking of UV light by CND-films.

fluorescent inks. A QR code pattern printed using an aqueous solution of CNDs is colorless under natural light but fluorescent blue under 365 nm UV light, allowing the hidden information to be readily accessed using a mobile phone (Fig. 3a). The QR code can still be rapidly read after 5 h irradiation with 365 nm UV light (Fig. 3a and Video S1†). These results further indicate that aqueous solutions of CNDs have good resistance to photobleaching and can be used as stable fluorescent inks.

Building on the observed concentration correlativity and optical stability of the fluorescence emission of solutions of CNDs, we next prepared CND-films containing different proportions of CNDs by compounding the CNDs with PVA. As the proportion of CNDs was increased, the CND-film changed from colorless to brown under natural light because of the color of the CNDs (Fig. 3b top panel and Fig. S7†). Scanning electron microscopy (SEM) images showed that the surface of the prepared CND-films was smooth and that the thickness of the films ranged from 37 μm to 44 μm (Fig. S8†). The stress–strain curves of PVA film and CND-film (Fig. S9 and Video S3†) showed that the maximum fracture strain and toughness of CND-film were significantly higher than those of pure PVA film, which is attributed to the strong hydrogen bonding between CNDs and PVA.[58,59] The transmittance of violet and blue light (≤450 nm) by pure PVA film exceeds 90% (Fig. 3c). The transmittance of ≤450 nm light by CND-films gradually decreases as the proportion of CNDs in the film is increased, especially for UV-C (230–280 nm) and UV-B (280–315 nm) and UV-A (315–400 nm), which also have more obvious blocking ability whereas there is little change in the transmittance of >800 nm visible light (Fig. 3c). This is because CNDs in the CND-film can absorb short wavelength light and convert it into longer wavelength emission; the higher the proportion of CNDs in the CND-film, the stronger its ability to convert incident light to longer wavelength emission. As the proportion of CNDs in the CND-film increases, the fluorescent color of CND-film can be seen to change from colorless to blue to yellow-green at 365 nm (Fig. 3b bottom panel). The ability of the CND-film to absorb short wavelength light and convert it into longer wavelength emission is thus related to the proportion of CNDs in the CND-film. These results indicate that the CND-films may have potential applications in blocking UV and high-energy blue photons.[1,2,6,10] To further investigate the light absorption and conversion characteristics of the CND-films, a 365 nm semiconductor chip (purple) was selected as the excitation source and different CND-films were used to encapsulate the chip (Fig. 3d). As the proportion of CNDs was increased, the film transformed 365 nm incident light into long wavelength emission, resulting in blue to orange LEDs (Fig. 3d and e). Since blue and yellow-green (or yellow) light can combine to produce white light, a WLED with pure white light can be obtained by superimposing CND-films containing 32 wt% and 16 wt% CNDs, using a 450 nm (blue) semiconductor chip as the excitation source (Fig. S10a† inset). The CIE1931 chromaticity coordinates, correlated color temperature and color rendering index were (0.3570, 0.3527), 4568 K and 83.8, respectively (Fig. S10a†). The electroluminescence spectrum of the WLED is shown in Fig. S10b.† These results further demonstrate the ability of CND-films to absorb short wavelength light and convert it into long wavelength emission. To further investigate the ability of CND-films to absorb short wavelength light and convert it into long wavelength emission, the normalized emission spectra of CND-films under light excitation at 365 nm, 405 nm and 450 nm were recorded (Fig. 4a–c). As the proportion of CNDs increased, the CND-films converted absorbed short wavelength light to

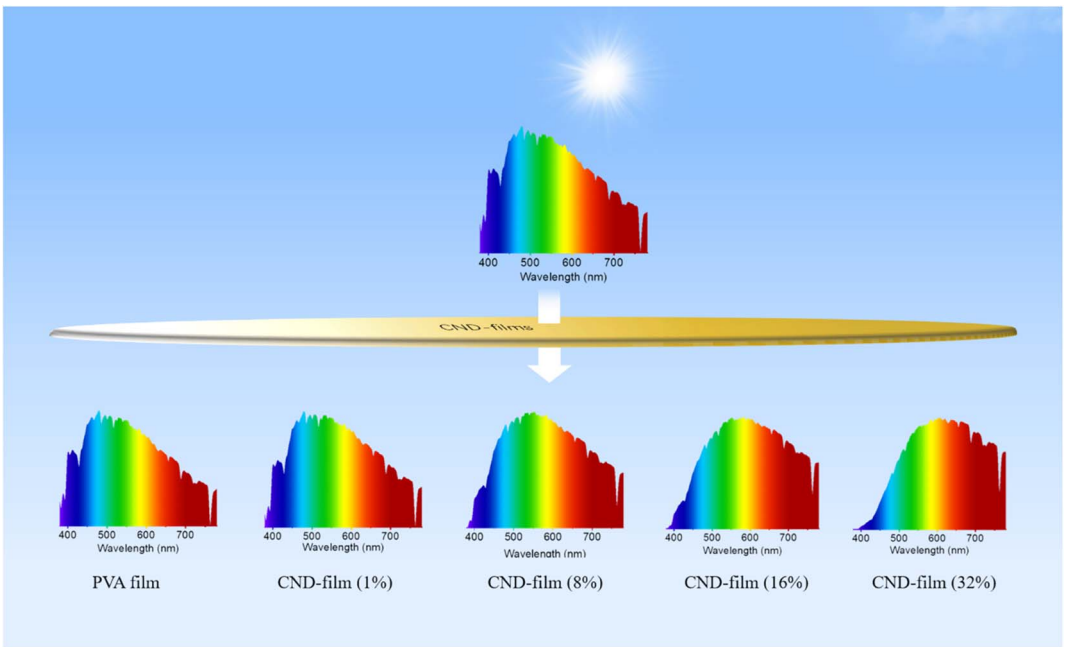

Fig. 5 Intensity spectra comparing blocking of solar UV light by PVA film and CND-films (1–32 wt%).

longer wavelength emission and the CIE1931 coordinates also showed red-shifted color changes (Fig. 4d–f). All of the above results confirm that CND-films containing different proportions of CNDs have different abilities to convert short wavelength light into long wavelength emission. To assess the practical ability of CND-films to block UV rays from sunlight, their ability to block UV rays (≤400 nm) in outdoor sunlight was measured. As the proportion of CNDs in the film increased, the intensity of UV radiation passing through the CND-films gradually decreased (Fig. 4g) and extent of UV blocking gradually increased (Fig. 4h). The UV blocking mechanism of CND-film can be summarized as follows: high-energy short wavelength light in sunlight is absorbed by the CND units in the CND-film and converted into long wavelength emission, thus effectively preventing damage caused by short wavelength light (Fig. 4i). When the proportion of CNDs was 32 wt%, the CND-film completely blocked the UV rays in sunlight (Fig. 5) and also blocked the direct incidence of a large amount of high-energy blue light (Fig. 5). A commercially available UV-induced color change card showed that whereas pure PVA has next to no ability to block UV rays from sunlight, the ability of CND-films to block UV rays becomes stronger and stronger as the proportion of CNDs in the film increases (Video S2†). The CNDs-films can not only block UV light, but also maintain good transparency,[60–62] and also reduce the doping amount of CNDs,[2] compared with the reported UV-blocking film. These results confirm that CNDs with concentration-dependent emission can be used as optical barrier units in materials designed to block high-energy short wavelength light.

Conclusions

In summary, CNDs with concentration-dependent emission and a high PLQY (45%) were synthesized in one step from sustainable chitosan resources. Aqueous solutions of the CNDs showed good temperature responsiveness and cyclability, as well as good stability against photobleaching. A "QR code" printed using a solution of CNDs, which was invisible under natural light, could be quickly identified under 365 nm light using a mobile phone and remained visible even after 5 h exposure to 365 nm irradiation, demonstrating that solutions of CNDs can be used as stable fluorescent inks. Transparent CND-films containing different proportions of CNDs were obtained by mixing the CNDs with PVA. These films block short wavelength light (≤450 nm), suggesting that they can be used to block UV and high-energy blue light. CND-films can efficiently block the transmission of short wavelength light (≤450 nm), without affecting or weakening visible light (>800 nm). As the proportion of CNDs in the film increased, the intensity of transmitted UV light (≤400 nm) gradually decreased and the extent of UV blocking by the CND-film gradually increased. When the proportion of CNDs reached 32 wt%, UV light in sunlight was completely blocked. Moreover, using a commercially available UV-induced color change card test, it could be clearly seen that pure PVA film does not block UV light whereas CND-films have a marked ability to block the UV component of sunlight. This study shows that CNDs with concentration-dependent emission can be used as optical barrier units for the preparation of materials to block high-energy short wavelength light.

Data availability

ESI data† can be found in the online version of the paper.

Conflicts of interest

The authors declare that they have no competing financial interests or personal relationships that could have influenced the work reported in this paper.

Acknowledgements

This work was supported by the National Natural Science Foundation of China (32171715), the Natural Science Foundation of Heilongjiang Province (LH2022C012) and the Hei Long Jiang Postdoctoral Foundation (LBH-Q21003). The authors are grateful for the funding.

Notes and references

1 H. Guo, X. Zhang, Z. Chen, L. Zhang, L. Wang, J. Xu and M. Wu, *Carbon*, 2022, **199**, 431–438.
2 S. J. Park, H. K. Yang and B. K. Moon, *Nano Energy*, 2019, **60**, 87–94.
3 G. Supanakorn, R. Thiramanas, T. Mahatnirunkul, Y. Wongngam and D. Polpanich, *ACS Appl. Nano Mater.*, 2022, **5**, 9084–9095.
4 Y. Wang, H. Deng and J. Kan, *Sci. Technol. Food Ind.*, 2013, **34**, 142.
5 F. C. John, K. Morris, R. B. Jordan and B. Thomas, hyphen and hyphen, *J. Exp. Bot.*, 2001, **52**, 1367–1373.
6 L. Zhao, M. Zhang, A. S. Mujumdar, B. Adhikari and H. Wang, *ACS Appl. Mater. Interfaces*, 2022, **14**, 37528–37539.
7 H. Guo, D. Klose, Y. Hou, G. Jeschke and I. Burgert, *ACS Appl. Mater. Interfaces*, 2017, **9**, 39040–39047.
8 Q. Xia, C. Chen, Y. Yao, S. He, X. Wang, J. Li, J. Gao, W. Gan, B. Jiang, M. Cui and L. Hu, *Adv. Mater.*, 2021, **33**, e2001588.
9 I. Rabani, H. N. Jang, Y. J. Park, M. S. Tahir, Y. B. Lee, E. Y. Moon, J. W. Song and Y. S. Seo, *RSC Adv.*, 2022, **12**, 33653–33665.
10 Y. Han, Y. Wang, B. Zhao, Y. Bai, S. Han, Y. Zhang, S. Li, Z. Chen, C. Si, H. Yu, C. Zhang and W. Yu, *Adv. Compos. Hybrid Mater.*, 2023, **6**, 39.
11 Y. Han, X. Huang, J. Liu, J. Ni, Y. Bai, B. Zhao, S. Han and C. Zhang, *J. Colloid Interface Sci.*, 2022, **617**, 44–52.
12 L. Ai, Z. Song, M. Nie, J. Yu, F. Liu, H. Song, B. Zhang, G. I. N. Waterhouse and S. Lu, *Angew. Chem., Int. Ed. Engl.*, 2023, **62**, e202217822.
13 A. Doring, E. Ushakova and A. L. Rogach, *Light: Sci. Appl.*, 2022, **11**, 75.
14 B. Wang, G. I. N. Waterhouse and S. Lu, *Trends Chem.*, 2023, **5**, 76–87.

15 D. Li, Y. Qu, X. Zhang, W. Zheng, A. L. Rogach and S. Qu, *Chem. Eng. J.*, 2023, **454**, 140069.
16 L. Wang, L. Li, B. Wang, J. Wu, Y. Liu, E. Liu, H. Zhang, B. Zhang, G. Xing, Q. Li, Z. Tang, C. Deng and S. Qu, *Small*, 2023, e2206667, DOI: 10.1002/smll.202206667.
17 J. Ni, X. Huang, Y. Bai, B. Zhao, Y. Han, S. Han, T. Xu, C. Si and C. Zhang, *Adv. Compos. Hybrid Mater.*, 2022, **5**, 1865–1875.
18 P. Ma, X. Sun, W. Pan, G. Yu and J. Wang, *ACS Sustainable Chem. Eng.*, 2020, **8**, 3151–3161.
19 X. Liu, L. Yan, J. Zheng, Y. Yang, X. Liu and B. Xu, *J. Mater. Chem. C*, 2023, **11**, 3562–3570.
20 R. Kumari, A. Kumar, K. Negi and S. K. Sahu, *ACS Appl. Nano Mater.*, 2023, **6**, 918–929.
21 M. Ge, Y. Han, J. Ni, Y. Li, S. Han, S. Li, H. Yu, C. Zhang, S. Liu, J. Li and Z. Chen, *Chem. Eng. J.*, 2021, **413**, 127457.
22 Y. Liu, X. Kang, Y. Xu, Y. Li, S. Wang, C. Wang, W. Hu, R. Wang and J. Liu, *ACS Appl. Mater. Interfaces*, 2022, **14**, 22363–22371.
23 J. Zhou, M. Ge, Y. Han, J. Ni, X. Huang, S. Han, Z. Peng, Y. Li and S. Li, *ACS Omega*, 2020, **5**, 11842–11848.
24 Q. Zhang, F. Wang, R. Wang, J. Liu, Y. Ma, X. Qin and X. Zhong, *Adv. Sci.*, 2023, **10**, e2207566.
25 F.-J. Cao, L. Wang, C.-L. Feng, X. Lin and H. Feng, *RSC Adv.*, 2021, **11**, 34174–34180.
26 Y.-Q. Zhang, D.-K. Ma, Y.-G. Zhang, W. Chen and S.-M. Huang, *Nano Energy*, 2013, **2**, 545–552.
27 S. Zhang, M. Gao, Y. Zhai, J. Wen, J. Yu, T. He, Z. Kang and S. Lu, *J. Colloid Interface Sci.*, 2022, **622**, 662–674.
28 Q. Zhang, R. Wang, B. Feng, X. Zhong and K. K. Ostrikov, *Nat. Commun.*, 2021, **12**, 6856.
29 L. Bai, H. Yan, Y. Feng, W. Feng and L. Yuan, *Chem. Eng. J.*, 2019, **373**, 963–972.
30 D. Zhao, Y. Zhu, W. Cheng, W. Chen, Y. Wu and H. Yu, *Adv. Mater.*, 2021, **33**, e2000619.
31 W.-T. Cao, F.-F. Chen, Y.-J. Zhu, Y.-G. Zhang, Y.-Y. Jiang, M.-G. Ma and F. Chen, *ACS Nano*, 2018, **12**, 4583–4593.
32 C. Lu, C. Wang, J. Yu, J. Wang and F. Chu, *ChemSusChem*, 2020, **13**, 893–902.
33 T. Xu, H. Du, H. Liu, W. Liu, X. Zhang, C. Si, P. Liu and K. Zhang, *Adv. Mater.*, 2021, **33**, e2101368.
34 T. C. Wareing, P. Gentile and A. N. Phan, *ACS Nano*, 2021, **15**, 15471–15501.
35 B. Xue, Y. Yang, Y. Sun, J. Fan, X. Li and Z. Zhang, *Int. J. Biol. Macromol.*, 2019, **122**, 954–961.
36 W. Yang, Z. Mei, S. Feng, C. Li, J. Guo, H. Bian, H. Xiao, H. Dai, C. Hu and J. Han, *ACS Sustainable Chem. Eng.*, 2023, **11**, 10172–10182.
37 L. Bai, T. Kamarainen, W. Xiang, J. Majoinen, J. Seitsonen, R. Grande, S. Huan, L. Liu, Y. Fan and O. J. Rojas, *ACS Nano*, 2020, **14**, 6921–6930.
38 L. Bai, L. Liu, M. Esquivel, B. L. Tardy, S. Huan, X. Niu, S. Liu, G. Yang, Y. Fan and O. J. Rojas, *Chem. Rev.*, 2022, **122**, 11604–11674.
39 N. Hasheminejad, F. Khodaiyan and M. Safari, *Food Chem.*, 2019, **275**, 113–122.
40 H. Zhu, Y. Wang, M. Qu, Y. Pan, G. Zheng, K. Dai, M. Huang, A. Alhadhrami, M. M. Ibrahim, Z. M. El-Bahy, C. Liu, C. Shen and X. Liu, *Adv. Compos. Hybrid Mater.*, 2022, **5**, 1966–1975.
41 J. Tan, Q. Li, S. Meng, Y. Li, J. Yang, Y. Ye, Z. Tang, S. Qu and X. Ren, *Adv. Mater.*, 2021, **33**, e2006781.
42 D. Ozyurt, S. Shafqat, T. T. Pakkanen, R. K. Hocking, A. Mouritz and B. Fox, *Carbon*, 2021, **175**, 576–584.
43 X. Miao, D. Qu, D. Yang, B. Nie, Y. Zhao, H. Fan and Z. Sun, *Adv. Mater.*, 2018, **30**, 1704740.
44 Y. Hu, R. Guan, S. Zhang, X. Fan, W. Liu, K. Zhang, X. Shao, X. Li and Q. Yue, *Food Chem.*, 2022, **372**, 131287.
45 Y. Wu, H. Zhang, A. Pan, Q. Wang, Y. Zhang, G. Zhou and L. He, *Adv. Sci.*, 2019, **6**, 1801432.
46 J. Guo, H. Li, L. Ling, G. Li, R. Cheng, X. Lu, A.-Q. Xie, Q. Li, C.-F. Wang and S. Chen, *ACS Sustainable Chem. Eng.*, 2019, **8**, 1566–1572.
47 C. Ma, W.-T. Cao, W. Zhang, M.-G. Ma, W.-M. Sun, J. Zhang and F. Chen, *Chem. Eng. J.*, 2021, **403**, 126438.
48 R. Jalili, A. Khataee, M. R. Rashidi and A. Razmjou, *Food Chem.*, 2020, **314**, 126172.
49 Z. Wang, Y. Liu, S. Zhen, X. Li, W. Zhang, X. Sun, B. Xu, X. Wang, Z. Gao and X. Meng, *Adv. Sci.*, 2020, **7**, 1902688.
50 L. Jiang, H. Ding, S. Lu, T. Geng, G. Xiao, B. Zou and H. Bi, *Angew. Chem., Int. Ed. Engl.*, 2020, **59**, 9986–9991.
51 R. Dai, X. Chen, N. Ouyang and Y. Hu, *Chem. Eng. J.*, 2022, **431**, 134172.
52 Y. Chen, M. Zheng, Y. Xiao, H. Dong, H. Zhang, J. Zhuang, H. Hu, B. Lei and Y. Liu, *Adv. Mater.*, 2016, **28**, 312–318.
53 M. Ge, X. Huang, J. Ni, Y. Han, C. Zhang, S. Li, J. Cao, J. Li, Z. Chen and S. Han, *Dyes Pigm.*, 2021, **185**, 108953.
54 S. Bhattacharyya, F. Ehrat, P. Urban, R. Teves, R. Wyrwich, M. Doblinger, J. Feldmann, A. S. Urban and J. K. Stolarczyk, *Nat. Commun.*, 2017, **8**, 1401.
55 T. Zhang, F. Zhao, L. Li, B. Qi, D. Zhu, J. Lu and C. Lu, *ACS Appl. Mater. Interfaces*, 2018, **10**, 19796–19805.
56 Q. Ran, X. Wang, P. Ling, P. Yan, J. Xu, L. Jiang, Y. Wang, S. Su, S. Hu and J. Xiang, *Carbon*, 2022, **193**, 404–411.
57 X. Tao, M. Liao, F. Wu, Y. Jiang, J. Sun and S. Shi, *Chem. Eng. J.*, 2022, **443**, 136442.
58 K. Liu, W. Liu, W. Li, Y. Duan, K. Zhou, S. Zhang, S. Ni, T. Xu, H. Du and C. Si, *Adv. Compos. Hybrid Mater.*, 2022, **5**, 1078–1089.
59 Y. Li, H. Chen, Y. Dong, K. Li, L. Li and J. Li, *Ind. Crops Prod.*, 2016, **82**, 133–140.
60 Z. Chang, S. Zhang, F. Li, Z. Wang, J. Li, C. Xia, Y. Yu, L. Cai and Z. Huang, *Chem. Eng. J.*, 2021, **404**, 126505.
61 J. Li, S. Jiang, Y. Wei, X. Li, S. Q. Shi, W. Zhang and J. Li, *Composites, Part B*, 2021, **211**, 108645.
62 W. Yang, Y. Gao, C. Zuo, Y. Deng and H. Dai, *Carbohydr. Polym.*, 2019, **223**, 115050.